Ultrathin Limit of Exchange Bias Coupling at Oxide Multiferroic/Ferromagnetic Interfaces

M. Huijben, P. Yu, L. W. Martin, H. J. A. Molegraaf, Y.-H. Chu, M. B. Holcomb, N. Balke, G. Rijnders, and R. Ramesh*

The ability to create atomically perfect, lattice-matched heterostructures of complex perovskite oxides using state-of-the-art thin film growth techniques has generated new physical phenomena at engineered interfaces. The emergence of interesting behavior at interfaces between materials with coupled spin and charge degrees of freedom is fascinating from a fundamental perspective as well as for applications. In particular, the control of ferromagnetism with an electric field could lead to new applications in magnetic data storage, spintronics, and high-frequency magnetic devices which do not require large currents and magnetic fields for operation. In turn, such modalities of operation may pave a pathway for lower power/energy devices and smaller feature sizes.[1–3] Multiferroics, such as $BiFeO_3$ (BFO), which simultaneously exhibit multiple order parameters such as magnetism and ferroelectricity, offer an exciting way of coupling phenomena by utilizing the intrinsic magnetoelectric coupling in such materials in which the electric polarization is controlled by applied magnetic fields or magnetism by applied electric fields.[4–7] BFO is an antiferromagnetic, ferroelectric multiferroic with a Curie temperature of 820 °C and a Néel temperature of 370 °C,[8,9] which makes it appealing for room temperature applications. Various studies have focused on the control of the ferroelectric domain structure, the domain switching mechanisms and the coupling between ferroelectric and magnetic order parameters in BFO.[10]

Another pathway to magnetoelectric control is the utilization of two different types of coupling in a heterostructure. The intrinsic magnetoelectric coupling in a multiferroic material, such as BFO, will allow for electrical control of antiferromagnetism, while subsequently the extrinsic exchange coupling between this antiferromagnet and an adjacent ferromagnetic material will create new functionalities. Exchange anisotropy, or bias, describes the phenomena associated with the exchange interactions at the interface between an antiferromagnet and a ferromagnet. Exchange bias has been used in a wide variety of applications including permanent magnets, recording media, and domain stabilizers in recording heads based on anisotropic magnetoresistance.[11] Exchange bias heterostructures based on multiferroic materials, including $YMnO_3$,[12–14] and BFO,[15–18] have shown that strong exchange interactions can be demonstrated in a static manner using multiferroic antiferromagnets. Switching of local ferromagnetism with an applied electric field has been demonstrated for heterostructures based on metallic ferromagnets (i.e., $Co_{0.9}Fe_{0.1}$ or $Ni_{0.81}Fe_{0.19}$) and multiferroics such as BFO[19,20] and $YMnO_3$.[21]

Recently, reversible electric control of exchange bias was also shown for an all oxide heterostructure consisting of BFO and $La_{0.7}Sr_{0.3}MnO_3$ (LSMO),[22,23] where epitaxial growth gives rise to a coherent chemical structure across the interface that can greatly enhance the nature of the coupling. The physical properties of the BFO-LSMO interface have been studied in detail to demonstrate a local ferromagnetic state related to electronic orbital reconstruction[24] as well as an antiferrodistortive phase transition.[25] The atomic control of the interface determines the interfacial coupling and, therefore, strongly influences the bulk ferroelectric polarization in the thin film.[26] However, so far, the size limits to such interfacial coupling, both on the ferromagnet and the antiferromagnet side, is lacking. Particularly, the co-evolution of ferroelectricity and antiferromagnetism in the BFO and their influence on the magnetic coupling at the interface remains unexplored. This is the central focus of this study.

Dr. M. Huijben, Dr. H. J. A. Molegraaf,
Prof. G. Rijnders
MESA+ Institute for Nanotechnology
University of Twente
P.O. BOX 217, 7500 AE, Enschede
The Netherlands
E-mail: m.huijben@utwente.nl

Dr. P. Yu
State Key Laboratory for Low-Dimensional Quantum Physics
Department of Physics
Tsinghua University
Beijing, China

Dr. L. W. Martin
Department of Materials Science and Engineering
and Materials Research Laboratory
University of Illinois
Urbana, IL 61801, USA

Dr. Y.-H. Chu
Department of Materials Science and Engineering
National Chiao Tung University
Hsinchu 30010, Taiwan

Dr. M. B. Holcomb
Physics Department
West Virginia University
P.O. Box 6315, Morgantown, WV 26506, USA

Dr. N. Balke
The Center for Nanophase Materials Sciences
Oak Ridge National Laboratory
Oak Ridge, TN 37831, USA

Prof. R. Ramesh
Departments of Materials Science and Engineering and Physics
University of California
Berkeley and Materials Science Division
Lawrence Berkeley National Laboratory
Berkeley, CA 94720, USA

DOI: 10.1002/adma.201300940

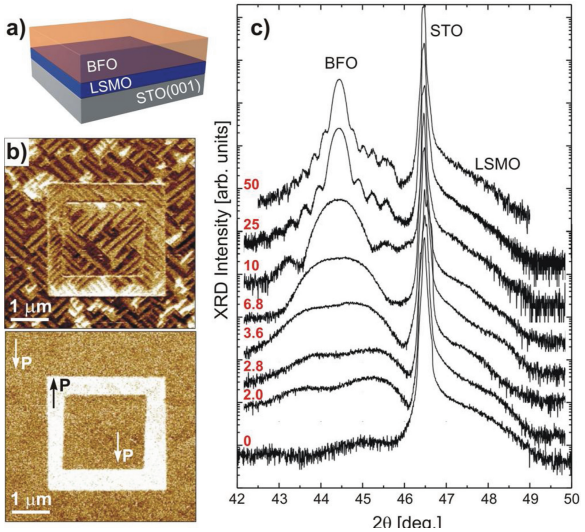

Figure 1. (a) Schematic of the BFO/LSMO/STO(001) heterostructure. (b) In-plane and out-of-plane PFM images (top and bottom panel, respectively) showing the ferroelectric domain structure of a BFO film with a large and small subsequently electrically switched region. (c) X-ray diffraction analysis of BFO/LSMO (5 nm) heterostructures with varying BFO thicknesses from 2 to 50 nm. Scans are shifted for clarity.

Here, we have used the concept of oxide heteroepitaxy for creating such artificially engineered interfaces to determine the critical limit of the individual multiferroic and ferromagnetic materials for generating interfacial exchange bias coupling. Aided by in situ monitoring of the growth, high-quality, atomically precise heterointerfaces have been produced with unit cell control of the respective multiferroic and ferromagnet layer thicknesses. Systematic analysis of the magnetic hysteresis loops allowed us to detect exchange bias coupling down to 5 unit cells (2.0 nm) in epitaxial BFO films.

Heterostructures of the ferromagnet LSMO and the multiferroic BFO were fabricated by pulsed-laser deposition while monitoring the growth process by reflection high-energy electron diffraction (RHEED) (**Figure 1**a) (see the Experimental Section for the deposition parameters). The surface structure and underlying ferroelectric domain structure were analyzed using piezoresponse force microscopy (PFM) and indicated the presence of stripe-like ferroelectric domains in films thicker than 30 nm (separated by 71° domain walls) in the BFO (Figure 1b) as shown in previous studies.[27,28] The polarization of the as-grown BFO layer was oriented downwards. The polarization in all BFO films, from 50 nm down to 2.0 nm, was found to be repeatedly and reproducibly switchable.[29] Structural measurements by X-ray diffraction reveal single phase, fully epitaxial layers of LSMO and BFO, which were strained in-plane to the STO (001) substrate. Figure 1c shows the presence of Kiessig fringes alongside the BFO 002-diffraction peak indicating a highly ordered crystalline sample with a very smooth interface and surface. The atomic and chemical configuration at the BFO/LSMO interface was studied with high angle annular dark-field (HAADF) imaging and spatially-resolved electron energy-loss spectroscopy (EELS) in a scanning transmission electron microscope (STEM), not shown here. Detailed results demonstrated sharp interfaces with a local increase in the pseudo cubic *c* lattice parameter in the first few unit cells of BFO adjacent to the interface, indicating an antiferrodistortive phase transition.[25,30]

The magnetic properties are shown in **Figure 2**a with a typical magnetization curve at 10 K for a 25 nm BFO/5 nm LSMO heterostructure with the magnetic field (B) applied along the [100] direction of the heterostructure after magnetic field cooling from above the T_C of the LSMO (360 K) to 10 K at +1 Tesla (red) and −1 Tesla (blue). As a comparison, the magnetization curve of a single 5 nm LSMO layer (black) is also shown.[31] The BFO/LSMO heterostructure exhibits, at low temperatures, a clear enhancement of the coercive field (H_C ≈150 Oe) as compared to a single LSMO layer (H_C ≈40 Oe) on STO (001) substrates and a ≈|40| Oe shift of the hysteresis loop (exchange bias) is also observed. The shift of the hysteresis loop is opposite to the direction of the cooling field, as expected from conventional exchange bias behavior, and suggests ferromagnetic alignment between the pinned, uncompensated spins in the antiferromagnet and the spins of the ferromagnet.[11,32] An alternative mechanism, driven by the intrinsic Dzyaloshinskii-Moriya interaction and ferroelectric polarization, has also been reported.[33] More detailed analyses of the temperature dependence of the observed coercive field (H_C) enhancement and exchange bias shift (H_{EB}) are given

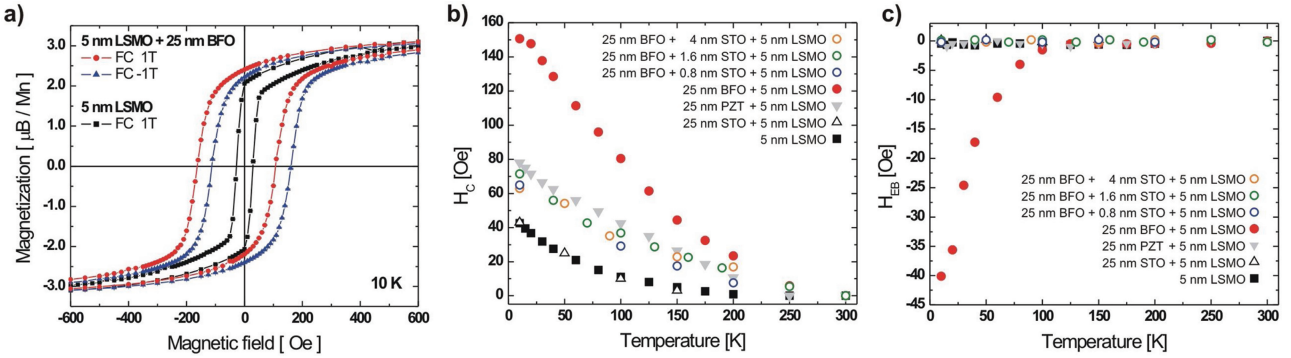

Figure 2. (a) Magnetic hysteresis loops of a BFO/LSMO heterostructure and a single LSMO layer measured along the [100] direction at 10 K after +/− 1 Tesla field cooling from 360 K. (b,c) Temperature dependences of the coercive field H_C enhancements and exchange bias shifts H_{EB} in BFO/LSMO, BFO/STO/LSMO, PZT/LSMO & STO/LSMO heterostructures and a single LSMO layer, respectively.

in Figure 2b and 2c, respectively. At higher temperatures the magnetic properties are determined by the thin (5 nm) LSMO layer and no difference can be observed between the heterostructures and the single layer. Although coercive field enhancement is visible for all cases below 250 K, the BFO/LSMO heterostructures show a much more drastic increase in H_C, which becomes a factor of 4 larger than the LSMO single layer at 10 K (Figure 2b).

To differentiate the role of strain, doping, and magnetic interactions in changing the coercive field, we have studied several types of heterostructures. The temperature dependence of the coercive field of a $PbZr_{0.2}Ti_{0.8}O_3$ (PZT)/LSMO heterostructure is shown in grey in Figure 2b. The PZT/LSMO heterostructure also shows an enhancement in H_C, compared to the single LSMO layer, consistent with prior studies.[34] It is, however, important to note that at all temperatures, the BFO/LSMO heterostructures show a larger H_C compared to the PZT/LSMO heterostructures, hinting at an additional contribution from magnetic interactions across the interface, as the effective polarization is similar in this direction. These BFO/LSMO heterostructures also exhibit a clear exchange bias shift, which vanishes above ≈100–120 K (Figure 2c), suggesting the existence of a blocking temperature,[11] which is significantly lower than the ferromagnetic T_C of the LSMO film (measured to be ≈320 K in these 5 nm thin films). It is interesting to note that this blocking temperature corresponds closely to the temperature above which spin polarization, as measured by photoemission, is lost in LSMO[35] as well as the vanishing of tunnel magnetoresistance in LSMO/STO/LSMO tunnel junctions.[36] Although exchange bias interactions are observed between LSMO and BFO, it is not present in the case of a single LSMO layer or PZT/LSMO heterostructure. The fact that the exchange bias shifts are only observed in heterostructures of the ferromagnet LSMO together with the ferroelectric/antiferromagnetic BFO and not with the ferroelectric PZT points to the integral role that the antiferromagnetic properties of the BFO play in determining the properties of such heterostructures.

In order to explore this further, we introduced a thin non-magnetic STO spacer layer of 2, 4, or 10 unit cells (0.8, 1.6, and 4 nm, respectively) in between the BFO and LSMO layers; in addition, we also prepared STO/LSMO heterostructures, with the BFO completely replaced by a similar thickness of STO. The results of these experiments on the coercive field as well as the exchange bias are included in Figure 2b and c. It is fascinating to note that even with only 2 unit cells of STO between the LSMO and BFO, the coercive field drops to a value very close to that observed for the LSMO/PZT heterostructure. Further increases of the STO thickness has a minimal further effect on the coercive field. Additionally, when the BFO is not present (i.e., a STO/LSMO heterostructure), we observe another drop in the coercive field to a value close to that of the pure LSMO layer. Most importantly, in all cases, we observe no exchange bias when a STO interlayer is present, clearly indicating that the non-magnetic STO layer has magnetically decoupled both layers and eliminated the contributions of uncompensated spins at the interface and prevents exchange bias coupling, see Figure 2c. The fact that there is a clear dependence of the exchange bias and coercive field as a function of the STO layer is interesting and is also consistent with prior work on the role of intermediary layers on exchange coupling in conventional exchange coupled systems.[37,38]

A clear thickness dependence of the exchange bias interactions in the BFO/LSMO heterostructures is observed as the thickness of the ferromagnetic LSMO layer is varied (**Figure 3**). The H_{EB} and H_C enhancement at 10 K are shown together with the magnetic transition temperature (T_C) for both the BFO/LSMO heterostructures and for single LSMO layers as a function of the LSMO layer thickness. The exchange bias field is inversely proportional to the thickness of the ferromagnetic layers, see inset in the top panel of Figure 3a, which is in good agreement with previous studies on conventional exchange bias systems.[11] For single LSMO layers down to a thickness of 5 nm the coercive field is very small and the transition temperature is above room temperature, see middle and bottom panel. When the LSMO thickness is decreased below 5 nm the coercive field as well as the transition temperature change drastically. This is generally interpreted by considering a strain-induced distortion of MnO_6 octahedra based on the Jahn-Teller distortion theory.[39] A recent study on ultrathin LSMO films has demonstrated bulk-like transport/magnetic properties down to a thickness of 5 nm before the metallic behavior progressively changed over to semiconducting (≈32 Å) and the disappearance of ferromagnetism (≈12 Å).[31]

It is important to note that the exchange bias coupling in BFO/LSMO heterostructures is fundamentally different from what has been reported in prior studies for metallic ferromagnets in contact with BFO.[17,18] For both cases (all oxide and oxide antiferromagnet-metallic ferromagnet heterostructures), studies on the (001) surface of BFO, which is a fully compensated surface, are expected to exhibit no exchange bias when minimal magnetic disorder as well as structural disorder[40] is present. Thus, another source of the pinned uncompensated spins is required to create exchange bias. In the case of heterostructures based on conventional ferromagnets [i.e., $Co_{0.9}Fe_{0.1}$ (CoFe)] that are exchange coupled to BFO, the ability to directly tune this exchange interaction by controlling the underlying domain structure of the BFO film has been observed.[17,18] By controlling the growth rate of the BFO layer, prior studies have shown the ability to make so called stripe-like (possessing predominantly 71° domain walls) and mosaic-like (possessing a large fraction of 109° domain walls) BFO films and a direct correlation between the magnitude of the exchange bias and the density of certain types of domain walls was observed.[18] This effect is not observed in these BFO/LSMO heterostructures. Regardless of the BFO domain structure, similar exchange bias shifts are observed at temperatures less than 120 K. This low temperature turn on of the exchange bias is yet another important difference between the BFO/LSMO heterostructures and the previously studied $Co_{0.9}Fe_{0.1}$/BFO system that points to a fundamental difference in the nature of exchange coupling. Temperature dependence studies of $Co_{0.9}Fe_{0.1}$/BFO heterostructures showed no observable change in the magnitude of exchange bias as a function of temperature from 300 to 10 K regardless of the underlying BFO domain structure. This difference can be ascribed to the presence of a local ferromagnetic state[24] at the BFO-LSMO interface as well as an antiferrodistortive phase transition.[25]

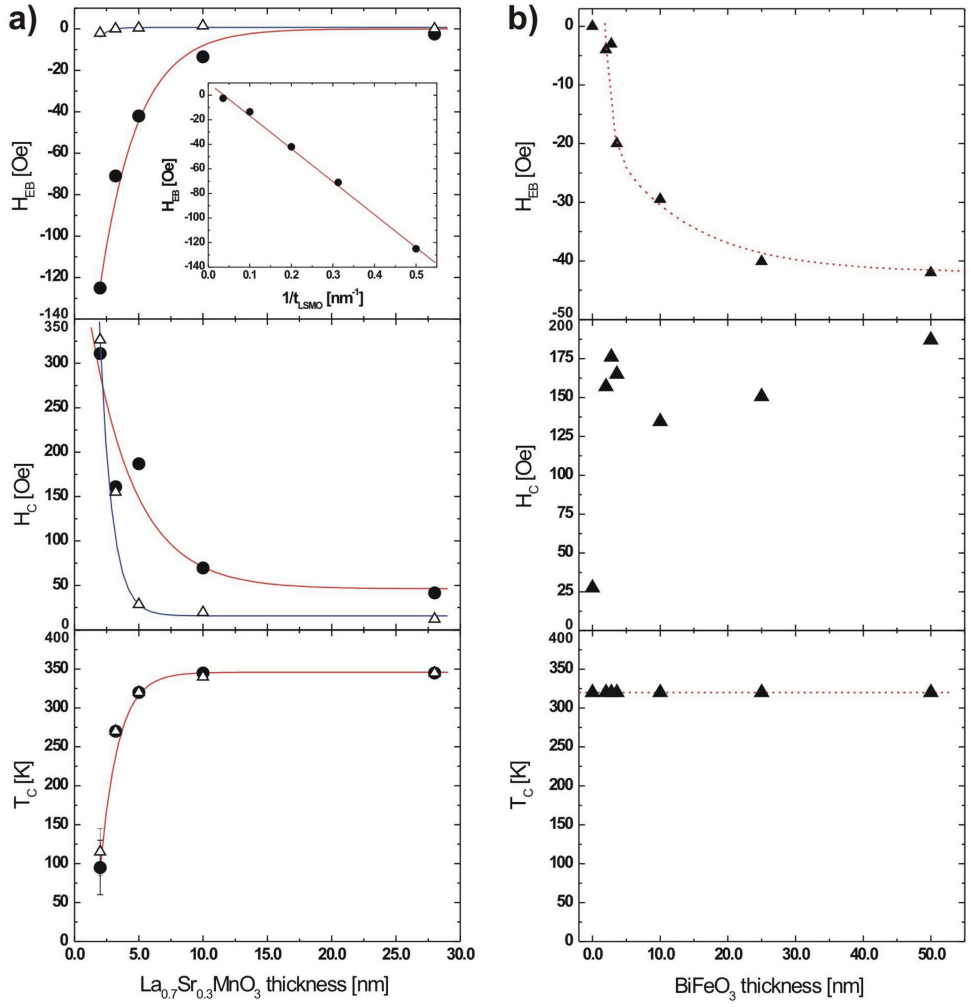

Figure 3. Thickness dependence of (a) the ferromagnetic LSMO layer and (b) the multiferroic BFO layer on the exchange bias shift H_{EB} at 10 K (top), coercive field H_C enhancement at 10 K (middle) and transition temperature T_C (bottom) for BFO/LSMO heterostructures with respectively (a) constant 50 nm BFO top-layer (black circles) and (b) constant 5 nm LSMO bottomlayer (black triangles). Data for single LSMO layers (open triangles) are also shown. The inset shows the inverse proportionality of the exchange bias shifts H_{EB} with the LSMO layer thickness. Lines are guides to the eye.

The theoretical expression for exchange bias coupling predicts that there is a critical thickness for the antiferromagnetic layer below which the exchange bias cannot exist.[41] Below this critical thickness the interfacial energy is transformed into coercivity. Above the critical thickness the exchange bias increases as a function of the antiferromagnetic layer thickness, reaching the asymptotic (ideal) value for exchange bias when the thickness is infinite. This has been experimentally demonstrated for conventional metallic systems[42–44] and can be qualitatively understood within the Meiklejohn and Bean model.[45] When the hardness of the antiferromagnetic layer is reduced, the antiferromagnetic spins will rotate under the torque created by the ferromagnetic layer through the interfacial magnetic coupling. The shape of the exchange bias as function of antiferromagnetic thickness, however, can be different from one system to another depending on the anisotropy of the antiferromagnet, the interfacial exchange coupling parameter and the interfacial ordering.[46]

Figure 3b shows a clear thickness dependence of the exchange bias coupling on the variations in thickness of the antiferromagnetic BFO layer. The exchange bias shift H_{EB} decreases monotonically with decreasing BFO layer thicknesses with the absence of any peak-like feature at the critical thickness. This has been theoretically modeled to result from a high conversion factor, i.e. high interfacial ordering,[46] which suggests a close to perfect BFO/LSMO interface with low disorder, in good agreement with STEM-EELS analysis of the interface.[25,30] In contrast to the exchange bias shift H_{EB}, the observed coercive field H_C remained high for all BFO thicknesses. As the magnetic transition temperature T_C is determined by the constant ferromagnetic LSMO layer of 5 nm, no variations are observed.

Experimentally it is found that a reduced antiferromagnetic BFO layer thickness will lower the blocking temperature below which exchange bias coupling occurs, see **Figure 4**. For a fixed antiferromagnetic layer thickness, there exists a critical value

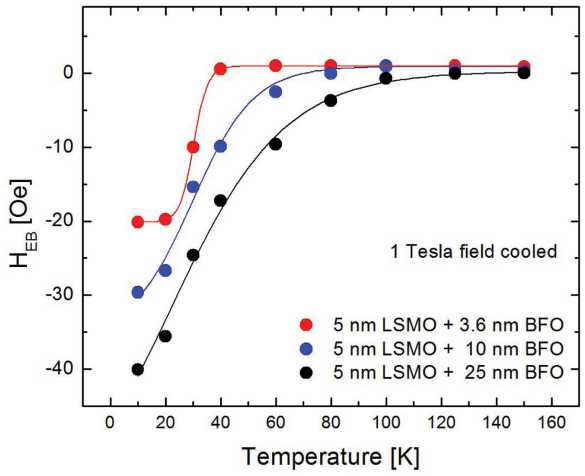

Figure 4. Temperature dependence of the exchange bias shift H_{EB} for BFO/LSMO heterostructures with various BFO layer thicknesses and a constant 5 nm LSMO bottomlayer. Lines are guides to the eye.

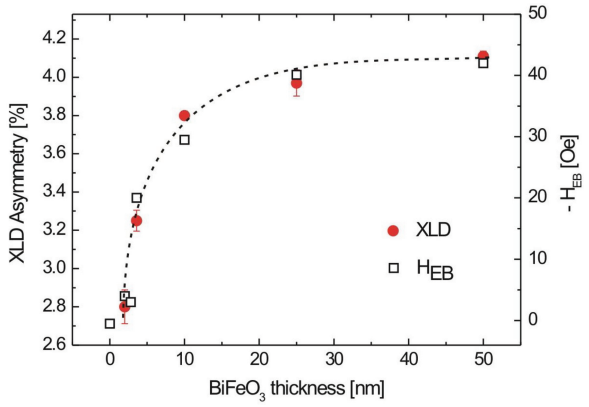

Figure 5. Experimental LD-XAS measurements at 17 K at the Fe-$L_{2,3}$ edge for BFO/LSMO heterostructures with BFO thicknesses between 2.0 and 50 nm. XLD asymmetry in percent of the XAS L_3 peak height signal, together with exchange bias shifts H_{EB}.

for the antiferromagnetic anisotropy for which the exchange bias coupling can exist.[11] Considering that the antiferromagnetic anisotropy increases steadily below the Néel temperature, this results in blocking temperatures of about 120 K for thick BFO layers. While for thinner BFO layers the critical value for the antiferromagnetic anisotropy is achieved at correspondingly lower temperatures. Figure 4 shows the decrease of the blocking temperature from 120 to 40 K when the BFO layer thickness is reduced from 25 to 3.6 nm.

X-ray absorption spectroscopy (XAS) spectra were recorded at the Fe-$L_{2,3}$ edge corresponding to the 2p to 3d dipole transition in order to study the evolution of antiferromagnetism in these ultrathin BFO films. The spin-orbit interaction of the Fe 2*p* core hole splits the spectrum into two broad multiplets, the L_3 ($2p_{3/2}$) edge at lower photon energy and the L_2 ($2p_{1/2}$) edge at higher photon energy. Using linearly polarized radiation, two spectra can be measured when the polarization vector is set parallel to the crystallographic *c*-axis or perpendicular to it (I_c and I_{ab}, respectively).[47] The difference between those spectra $(I_{ab} - I_c)/(I_{ab} + I_c)$ provides the linear dichroism (LD) values, which originates from anisotropies in the spin and charge of the material. In the case of BFO an additional ferroelectric contribution can be expected besides the antiferromagnetic order. However, previous characterization of the ferroelectric properties of these BFO/LSMO heterostructures have demonstrated the presence of a constant ferroelectric polarization in this BFO thickness range.[29] Therefore, analysis of linear dichroism in these heterostructures gives direct insight into the evolution of the antiferromagnetic ordering. LD-XAS measurements were performed on BFO/LSMO heterostructures with variable BFO layer thicknesses between 2 and 50 nm. The dependence of the linear dichroism, i.e., antiferromagnetic ordering, on the thickness of the BFO layer is shown in **Figure 5** together with the evolution of the exchange bias coupling. A close relationship between the enhanced antiferromagnetic ordering in the multiferroic BFO layers and the increasing exchange bias coupling can be observed for thicker BFO layers within the BFO/LSMO heterostructures.

In summary, we have studied exchange bias coupling in BFO/LSMO heterostructures for variable thicknesses of the individual multiferroic and ferromagnetic layers. For thick multiferroic BFO layers the exchange bias field is inversely proportional to the thickness of the ferromagnetic layers, which is in good agreement with previous studies on conventional exchange bias systems. Furthermore, for ultrathin multiferroic BFO layers a critical thickness of 2 nm, i.e., 5 unit cells, was determined below which the exchange bias cannot exist. As previous studies have shown that the ferroelectric polarization remains present in these BFO/LSMO heterostructures even down to BFO thicknesses of only 4 unit cells, the evolution in antiferromagnet behavior of the multiferroic BFO layer determines the interfacial exchange bias coupling. The dependence of the antiferromagnetic ordering on the BFO layer thickness was demonstrated by LD-XAS, which showed a strongly reduced linear dichroism for ultrathin BFO layers. In conclusion, an ultrathin limit of 2 nm was determined for the multiferroic BFO layer thickness, above which exchange bias coupling to the ferromagnetic LSMO layer will occur.

Experimental Section

Epitaxial heterostructures of the ferromagnet LSMO and the multiferroic BFO were grown by pulsed-laser deposition with variable layer thicknesses in the range of 2 to 50 nm. TiO_2-terminated $SrTiO_3$ (STO) (100) substrates have been used, which were prepared by a combined HF-etching/anneal treatment,[48] exhibiting an atomically smooth surface with clear unit-cell-height steps. All substrates had vicinal angles of ≈0.1°. Stoichiometric LSMO and BFO targets were ablated at a laser fluence of 1.5 J cm^{-2} and a repetition rate of 1 or 2 Hz for the growth of LSMO and BFO, respectively. During growth, the substrate was held at 750 °C in an oxygen environment at 200 mTorr for LSMO,[31] while for BFO the conditions were adjusted to 670 °C and 100 mTorr.[18] RHEED analysis demonstrated intensity oscillations indicating layer-by-layer growth mode for the total LSMO layer, while a transition from layer-by-layer growth to step-flow growth was observed during the initial growth of BFO. This resulted in a controlled, very low roughness surface without any island formation. This was supported by the continuous presence of only 2-dimensional spots in the corresponding RHEED patterns,

indicating a very well controlled growth to fabricate high-quality BFO/LSMO interfaces. After the growth, the heterostructures were slowly cooled to room temperature in 1 Atm. of oxygen at a rate of 5 °C/min to optimize the oxidation level. In order to probe the details of the coupling at the BFO/LSMO interface, we have inserted, in some heterostructures, epitaxial interlayers of nonmagnetic STO between the LSMO and the BFO layers with thicknesses varying between 2 and 10 unit cells. These STO interlayers were grown in layer-by-layer mode at 750 °C and 100 mTorr. Furthermore, $PbZr_{0.2}Ti_{0.8}O_3$ (PZT)/LSMO heterostructures have been fabricated as well at similar growth conditions. Analysis techniques, such as piezoresponse force microscopy (PFM) and X-ray diffraction (XRD), were used to demonstrate the surface topography, ferroelectric domain structure and crystallinity of the BFO/LSMO heterostructures. The magnetic properties have been measured in the temperature range 10–360 K with the magnetic field applied in-plane along the <100> of the STO substrate crystal using a Quantum Design SQUID Magnetometer (MPMS). Linear dichroism was investigated for several BFO/LSMO heterostructures by X-ray absorption spectroscopy (XAS) measurements at 17 K of the Fe-$L_{2,3}$ edge at the Advanced Light Source (Lawrence Berkeley National Laboratory) to directly probe the evolution of spin/charge anisotropies in ultrathin BFO films.

Acknowledgements

This work was supported by the Director, Office of Science, Office of Basic Energy Sciences, Materials Sciences and Engineering Division of the US Department of Energy under Contract No.DE-AC02-05CH11231. M. H. and G. R. acknowledge support by the Netherlands Organization for Scientific Research (NWO). L. W. M. acknowledges support from the Army Research Office under grant W911NF-10-1-0482.

Received: February 28, 2013
Revised: May 13, 2013
Published online: July 12, 2013

[1] M. Fiebig, *J. Phys. D: Appl. Phys.* **2005**, *38*, R123.
[2] N. A. Spaldin, M. Fiebig, *Science* **2005**, *309*, 391.
[3] W. Eerenstein, N. D. Mathur, J. F. Scott, *Nature* **2006**, *442*, 759.
[4] R. Ramesh, N. A. Spaldin, *Nature Mater.* **2007**, *6*, 21.
[5] L. W. Martin, S. P. Crane, Y. H. Chu, M. B. Holcomb, M. Gajek, M. Huijben, C. H. Yang, N. Balke, R. Ramesh, *J. Phys.-Condens. Mat.* **2008**, *20*, 434220.
[6] K. F. Wang, J. M. Liu, Z. F. Ren, *Adv. Phys.* **2009**, *58*, 321.
[7] J. Ma, J. Hu, Z. Li, C. W. Nan, *Adv. Mater.* **2011**, *23*, 1062.
[8] S. V. Kiselev, R. P. Ozerov, G. S. Zhdanov, *Sov. Phys. Dokl.* **1963**, *7*, 742.
[9] J. R. Teague, R. Gerson, W. J. James, *Solid State Commun.* **1970**, *8*, 1073.
[10] L. W. Martin, R. Ramesh, *Acta Mater.* **2012**, *60*, 2449.
[11] J. Nogues, I. K. Schuller, *J. Magn. Magn. Mater.* **1999**, *192*, 203.
[12] J. Dho, M. G. Blamire, *Appl. Phys. Lett.* **2005**, *87*, 252504.
[13] X. Mart, F. Sanchez, J. Fontcuberta, M. V. Garca-Cuenca, C. Ferrater, M. Varela, *J. Appl. Phys.* **2006**, *99*, 08P302.
[14] X. Mart, F. Sanchez, D. Hrabovsky, L. Fabrega, A. Ruyter, J. Fontcuberta, V. Laukhin, V. Skumryev, M. V. Garca-Cuenca, C. Ferrater, M. Varela, A. Vila, U. Lders, J. F. Bobo, *Appl. Phys. Lett.* **2006**, *89*, 032510.
[15] J. Dho, X. Qi, H. Kim, J. L. MacManus-Driscoll, M. G. Blamire, *Adv. Mater.* **2006**, *18*, 1445.
[16] H. Bea, M. Bibes, S. Cherifi, F. Nolting, B. Warot-Fonrose, S. Fusil, G. Herranz, C. Deranlot, E. Jacquet, K. Bouzehouane, A. Barthélémy, *Appl. Phys. Lett.* **2006**, *89*, 242114.
[17] H. Bea, M. Bibes, F. Ott, B. Dupe, X. Zhu, S. Petit, S. Fusil, C. Deranlot, K. Bouzehouane, A. Barthélémy, *Phys. Rev. Lett.* **2008**, *100*, 17204.
[18] L. W. Martin, Y. H. Chu, M. B. Holcomb, M. Huijben, P. Yu, S. J. Han, D. Lee, S. X. Wang, R. Ramesh, *Nano Lett.* **2008**, *8*, 2050.
[19] Y. H. Chu, L. W. Martin, M. B. Holcomb, M. Gajek, S. J. Han, Q. He, N. Balke, C. H. Yang, D. Lee, W. Hu, Q. Zhan, P. L. Yang, A. Fraile-Rodrguez, A. Scholl, S. X. Wang, R. Ramesh, *Nature Mater.* **2008**, *7*, 478.
[20] J. T. Heron, M. Trassin, K. Ashraf, M. Gajek, Q. He, S. Y. Yang, D. E. Nikonov, Y.-H. Chu, S. Salahuddin, R. Ramesh, *Phys. Rev. Lett.* **2011**, *107*, 217202.
[21] V. Laukhin, V. Skumryev, X. Marti, D. Hrabovsky, F. Sanchez, M. V. Garcia-Cuenca, C. Ferrater, M. Varela, U. Lüders, J. F. Bobo, J. Fontcuberta, *Phys. Rev. Lett.* **2006**, *97*, 227201.
[22] S. M. Wu, S. A. Cybart, P. Yu, M. D. Rossell, J. X. Zhang, R. Ramesh, R. C. Dynes, *Nature Mater.* **2010**, *9*, 756.
[23] S. M. Wu, S. A. Cybart, D. Yi, J. M. Parker, R. Ramesh, R. C. Dynes, *Phys. Rev. Lett.* **2013**, *110*, 067202.
[24] P. Yu, J. S. Lee, S. Okamoto, M. D. Rossell, M. Huijben, C. H. Yang, Q. He, J. X. Zhang, S. Y. Yang, M. J. Lee, Q. M. Ramasse, R. Erni, Y. H. Chu, D. A. Arena, C. C. Kao, L. W. Martin, R. Ramesh, *Phys. Rev. Lett.* **2010**, *105*, 27201.
[25] A. Y. Borisevich, H. J. Chang, M. Huijben, M. P. Oxley, S. Okamoto, M. K. Niranjan, J. D. Burton, E. Y. Tsymbal, Y. H. Chu, P. Yu, R. Ramesh, S. V. Kalinin, S. J. Pennycook, *Phys. Rev. Lett.* **2010**, *105*, 87204.
[26] P. Yu, W. Luo, D. Yi, J. X. Zhang, M. D. Rossell, C. H. Yang, L. You, G. Singh-Bhalla, S. Y. Yang, Q. He, Q. M. Ramasse, R. Erni, L. W. Martin, Y. H. Chu, S. Pantelides, S. J. Pennycook, R. Ramesh, *Proc. Natl. Acad. Sci. USA* **2012**, *109*, 9710.
[27] N. Balke, S. Choudhury, S. Jesse, M. Huijben, Y. H. Chu, A. P. Baddorf, L. Q. Chen, R. Ramesh, S. V. Kalinin, *Nature Nanotech.* **2009**, *4*, 868.
[28] C. T. Nelson, P. Gao, J. R. Jokisaari, C. Heikes, C. Adamo, A. Melville, S. H. Baek, C. M. Folkman, B. Winchester, Y. Gu, Y. Liu, K. Zhang, E. Wang, J. Li, L. Q. Chen, C. B. Eom, D. Schlom, X. Pan, *Science* **2011**, *334*, 968.
[29] P. Maksymovych, M. Huijben, M. Pan, S. Jesse, N. Balke, Y. H. Chu, H. J. Chung, A. Y. Borisevich, A. P. Baddorf, G. Rijnders, D. H. A. Blank, R. Ramesh, S. V. Kalinin, *Phys. Rev. B* **2012**, *85*, 014119.
[30] H. J. Chang, S. V. Kalinin, A. N. Morozovska, M. Huijben, Y. H. Chu, P. Yu, R. Ramesh, E. A. Eliseev, G. S. Svechnikov, S. J. Pennycook, A. Y. Borisevich, *Adv. Mater.* **2011**, *23*, 2474.
[31] M. Huijben, L. W. Martin, Y. H. Chu, M. B. Holcomb, P. Yu, G. Rijnders, D. H. A. Blank, R. Ramesh, *Phys. Rev. B* **2008**, *78*, 094413.
[32] H. Ohldag, A. Scholl, F. Nolting, E. Arenholz, S. Maat, A. T. Young, M. Carey, J. Sthör, *Phys. Rev. Lett.* **2003**, *91*, 017203.
[33] S. Dong, K. Yamauchi, S. Yunoki, R. Yu, S. Liang, A. Moreo, J.-M. Liu, S. Picozzi, E. Dagott, *Phys. Rev. Lett.* **2009**, *103*, 127201.
[34] I. Vrejoiu, M. Ziese, A. Setzer, P. D. Esquinazi, B. I. Birajdar, A. Lotnyk, M. Alexe, D. Hesse, *Appl. Phys. Lett.* **2008**, *92*, 152506.
[35] J. H. Park, E. Vescovo, H. J. Kim, C. Kwon, R. Ramesh, T. Venkatesan, *Nature* **1998**, *392*, 794.
[36] J. Z. Sun, L. Krusin-Elbaum, P. R. Duncombe, A. Gupta, R. B. Laibowitz, *Appl. Phys. Lett.* **1997**, *70*, 1769.
[37] N. J. Gökemeijer, T. Ambrose, C. L. Chien, N. Wang, K. K. Fung, *J. Appl. Phys.* **1997**, *81*, 4999.
[38] N. J. Gökemeijer, T. Ambrose, C. L. Chien, *Phys. Rev. Lett.* **1997**, *79*, 4270.
[39] A. J. Millis, T. Darling, A. Migliori, *J. Appl. Phys.* **1998**, *83*, 1588.

[40] W. Kuch, L. I. Chelaru, F. Offi, J. Wang, M. Kotsugi, J. Kirschner, *Nature Mater.* **2006**, *5*, 128.
[41] D. Mauri, E. Kay, D. Scholl, J. K. Howard, *J. Appl. Phys.* **1987**, *62*, 2929.
[42] H. Xi, R. M. White, *Phys. Rev. B* **2000**, *61*, 80.
[43] M. Ali, C. H. Marrows, M. Al-Jawad, B. J. Hickey, A. Misra, U. Nowak, K. D. Usadel, *Phys. Rev. B* **2003**, *68*, 214420.
[44] J. Kohlhepp, W. J. M. de Jonge, *Phys. Rev. Lett.* **2006**, *96*, 237201.
[45] W. H. Meiklejohn, C. P. Bean, *Phys. Rev.* **1956**, *102*, 1413.
[46] F. Radu, H. Zabel, in *Magnetic heterostructures* (Eds: H. Zabel, S. D. Bader), Springer-Verlag, Berlin Heidelberg **2008**, 97–184.
[47] M. B. Holcomb, L. W. Martin, A. Scholl, Q. He, P. Yu, C. H. Yang, S. Y. Yang, P. A. Glans, M. Valvidares, M. Huijben, J. B. Kortright, J. Guo, Y. H. Chu, R. Ramesh, *Phys. Rev. B* **2010**, *81*, 134406.
[48] G. Koster, B. L. Kropman, A. J. H. M. Rijnders, D. H. A. Blank, H. Rogalla, *App. Phys. Lett.* **1998**, *73*, 2920.